Available online at www.sciencedirect.com
ScienceDirect
Acta Materialia xxx (2009) xxx–xxx
Acta MATERIALIA
www.elsevier.com/locate/actamat

Effect of pre-existing shear bands on the tensile mechanical properties of a bulk metallic glass

Q.P. Cao [a,*], J.W. Liu [a], K.J. Yang [b], F. Xu [a], Z.Q. Yao [b], A. Minkow [b], H.J. Fecht [b,c], J. Ivanisenko [c], L.Y. Chen [a], X.D. Wang [a], S.X. Qu [d], J.Z. Jiang [a,*]

[a] *International Center for New-Structured Materials (ICNSM), Zhejiang University and Laboratory of New-Structured Materials, Department of Materials Science and Engineering, Zhejiang University, Hangzhou 310027, PR China*
[b] *Institute of Micro and Nanomaterials, University of Ulm, Albert-Einstein Allee 47, 89091 Ulm, Germany*
[c] *Forschungszentrum Karlsruhe, Institut für Nanotechnologie, 76021 Karlsruhe, Germany*
[d] *International Center for New-Structured Materials (ICNSM), Zhejiang University and Institute of Applied Mechanics, School of Aeronautics and Astronautics, Zhejiang University, Hangzhou 310027, PR China*

Received 29 June 2009; received in revised form 20 October 2009; accepted 21 October 2009

Abstract

Bulk $Zr_{64.13}Cu_{15.75}Ni_{10.12}Al_{10}$ metallic glass has been rolled at room temperature in two different directions, and the dependences of microstructure and tensile mechanical property on the degree of deformation and rolling directions have been investigated. No deformation-induced crystallization occurs except for shear bands. Shear band formation in conjugated directions is achieved in the specimen rolled in two directions, while rolling in one direction induces shear band formation only in a single direction. Pre-existing properly spaced soft inhomogeneities can stabilize shear bands and lead to tensile plastic strain, and the efficient intersection of shear bands in conjugated directions results in work-hardening behavior, which is further confirmed by in situ tensile scanning electron microscopic observation. Based on the experimental results obtained in two different specimen geometries and finite element analysis, it is deduced that a normal-stress-modified maximum shear stress criterion rather than a shear plane criterion can describe the conditions for the formation of shear bands in uniaxial tension.

Keywords: Metallic glasses; Rolling; Shear bands; Tension test; In situ SEM

1. Introduction

Bulk metallic glasses (BMGs) possess attractive mechanical properties, such as large elastic limit (2%), high strength and high hardness, compared with their crystalline counterparts and other classes of engineering materials [1]. However, one critical drawback of BMGs is their brittleness at room temperature, which limits their application as structural materials. Although monolithic BMGs exhibit significant plasticity under constrained loading, such as indentation, bending, rolling and compression with a low specimen aspect ratio [2–5], they usually show very little ductility in uniaxial tension, and unlimited propagation of shear banding leads to catastrophic failure along a single shear band [6,7]. Since room-temperature plastic deformation of metallic glasses occurs via the formation and propagation of shear bands, understanding the mechanisms to initiate, maintain and arrest flow on a shear band is the key to gaining insight into deformation mechanisms and ductilization of metallic glasses, which remains unclear. In the indentation experiments of metallic glasses, it has been found that shear band fields under a complex compressive stress state closely match those predicted by slip-line field theory [8,9]. Local satisfaction of the yield criterion at a local point cannot initiate a shear band, shear

* Corresponding authors. Tel.: +86 571 8795 2107; fax: +86 571 8795 1528.
E-mail addresses: caoqp@zju.edu.cn (Q.P. Cao), jiangjz@zju.edu.cn (J.Z. Jiang).

1359-6454/$36.00 © 2009 Acta Materialia Inc. Published by Elsevier Ltd. All rights reserved.
doi:10.1016/j.actamat.2009.10.032

banding only occurring when the yield strength is exceeded everywhere along a potential shear band path; this is the shear plane criterion [10]. Under uniaxial tension and compression conditions, however, there are still no published reports about the applicability of the shear plane criterion to the initiation of shear bands.

Significant progress has been made in recent years to improve the plasticity of BMGs. For example, heterogeneous microstructures have been designed by virtue of the interaction between a glass matrix and second-phase crystalline particles to limit the propagation of shear bands, and tensile ductility of the composites has been achieved [11,12]. Remarkable plasticity of pre-plastic BMGs deformed by cold rolling and surface shot-peening has also been obtained in bending or compression tests [13,14]. Yokoyama et al. [15] performed tensile testing on the cold-rolled specimens with 5–20% thickness reductions, and found that rolling can enhance tensile plastic elongation. This was proposed to be due to the competitive movement and intersection of shear bands in different systems. Meanwhile, Yokoyama et al. also found that the as-rolled specimens possessed relatively lower yield and fracture stresses in comparison with the as-cast specimen, indicating that work-softening rather than work-hardening existed. Note that, although they noticed that with a fixed rolling direction shear bands normally propagate only along a single direction and introducing shear bands with different orientations can enhance tensile ductility [13], intentional variation in the orientation of shear bands by changing the rolling direction was not adopted to further enhance the mechanical properties of BMGs.

The possibility of work hardening in metallic glasses is still a matter of debate. Takayama [16] had investigated the drawing behavior of $Pd_{77.5}Cu_6Si_{16.5}$ metallic glass wire and found that on the surface of drawn specimens two families of numerous shear bands appeared with rather regular intersections between them. The drawn specimens exhibited greater elongation and slightly higher fracture stress during subsequent tension tests, and final fracture stress of deformed specimen is considered to be determined by the competition between work softening by pre-introduced shear bands and work hardening by intersections of shear bands. Hagiwara et al. [17] observed similar phenomena in the mechanical response of highly drawn $Co_{72.5}Si_{12.5}B_{15}$ metallic glass wire. Therefore, the work-hardening phenomenon may be observed if the orientation of pre-introduced shear bands is appropriately tuned and the intersection of shear bands is greatly enhanced. The purpose of the present work was to systematically investigate shear band evolution and to understand how shear bands form in uniaxial tension, and the effect of rolling direction on the microstructure and tensile mechanical properties.

2. Experiments

Quaternary $Zr_{64.13}Cu_{15.75}Ni_{10.12}Al_{10}$ master alloy ingots were prepared by arc melting 99.9+% pure elemental Zr, Cu, Ni and Al together under a Ti-gettered argon atmosphere. To ensure homogeneity, the master ingots were inverted and remelted several times, and subsequently suck-cast into a water-cooled copper mold to form 1 mm thick plates with a width of 10 mm. The as-cast plate was hand-polished using 200, 600 and 1200 grit SiC paper successively to remove the thin crystalline surface layer caused by interaction with the mold. The final thickness of polished plates was reduced to about 0.8 mm, with the upper and lower surfaces being parallel. The polished plates were cut into rectangular blocks with different lengths (5 and 15 mm) for rolling. Prior to the rolling experiment, the side surfaces of the as-cast specimens were polished mechanically using diamond pastes to a mirror finish. The rolling apparatus consisted of two 100 mm diameter rollers. Covered by two stainless steel sheets of 1 mm original thickness, the specimen was rolled in one direction (1d-rolling, i.e. continuous rolling without changing direction) and two directions (2d-rolling, i.e. rotating 180° in the rolling (horizontal) plane after each rolling pass), respectively, as illustrated in Fig. 1, until the desired degree of deformation was obtained. The degree of deformation in cold-rolled specimens can be described by the rate of reduction of thickness [18,19], but in this work the degree of deformation was denoted by $\varepsilon = (h_0 - h)/h$ [20], where h_0 and h represent the specimen thicknesses before and after rolling, respectively. Many small deformation passes were used with a progressively narrowing gap between two rollers. The decrease in the gap during rolling was carefully controlled so that the strain rate was about $5.0 \times 10^{-3}\ s^{-1}$.

The microstructure of the as-cast and as-rolled $Zr_{64.13}Cu_{15.75}Ni_{10.12}Al_{10}$ specimens was examined by X-ray diffraction (XRD) using a Thermo ARL X-ray diffractometer with monochromatic Cu K_α radiation and by high-resolution transmission electron microscopy (HRTEM) using JEOL JEM-2010, Philips CM 200 and Technai G2 F30 Lorenz transmission electron microscopes. Thin foils for TEM of the as-cast specimen were prepared by twin-jet electropolishing using a solution of 10% perchloric acid in ethanol at a temperature of 238 K. TEM foils of the as-rolled specimens were prepared by a Hitachi FIB2000 focused ion beam machine. Thermal analyses of the specimens subjected to different ε were performed in a Perkin–Elmer Pyris Diamond differential scanning calorimeter under a flow of purified argon. The side surface morphology of the as-cast and as-rolled specimens was observed with a Motic optical microscope and a FEI Sirion 200 field-emission scanning electron microscope. In situ tensile deformation for the as-cast and as-rolled specimens with different ε was observed using a Leo-1550 scanning electron microscope (Zeiss Company, Germany). Limited by the maximum load for the used tension device (Kammrath & Weiss Company, Germany) in the scanning electron microscope, the specimens thicker than 0.5 mm were polished down to about 0.4–0.5 mm thickness and to a mirror finish using SiC paper and diamond paste, while the specimens less than 0.5 mm thick were just

Please cite this article in press as: Cao QP et al. Effect of pre-existing shear bands on the tensile mechanical properties of a bulk metallic glass. Acta Mater (2009), doi:10.1016/j.actamat.2009.10.032

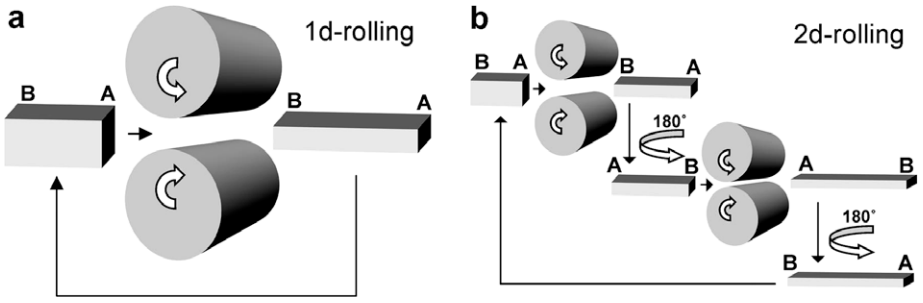

Fig. 1. Schematic illustration of (a) the 1d-rolling process and (b) the 2d-rolling process.

slightly polished to a mirror finish. The tensile stress was added by elongation controlled by a tunable extension rate to a strain rate of about 1.5×10^{-4} s^{-1}. Scanning electron microscopy (SEM) images were recorded at a given tensile stress during uniaxial tension. It should be noted that we only observed changes in situ on one side of the tensile specimen, as changes on the other side and in the interior of specimen could not be detected during tension. Since shear banding in metallic glasses occurs in the manner of a shear plane, however, the appearance of shear bands on one surface of the tensile specimen may represent the evolution of shear bands on the opposite surface and in the interior. Room-temperature tensile tests were also conducted using a dedicated tensile stage for miniature specimens on the as-cast and as-rolled specimens with the same shape as that for the SEM observation with a strain rate of 1.0×10^{-4} s^{-1}. Displacement was precisely directly measured on the sample gauge length using a laser extensometer developed by Fiedler Optoelektronik GmbH, Germany. At least three specimens were measured to ensure that the results were reproducible. Tension-induced stress distribution immediately prior to yield was investigated using the finite element method (ABAQUS 6.7-1).

3. Results and discussion

3.1. Microstructure of the as-cast and as-rolled specimens

The as-cast $Zr_{64.13}Cu_{15.75}Ni_{10.12}Al_{10}$ plate shows excellent rolling and bending capabilities, in good accordance with the results in Ref. [21]. The maximum degree of deformation achieved in 1d-rolling and 2d-rolling at room temperature both reach up to 1150%. Fig. 2a shows the outer pictures of the as-rolled specimens with $\varepsilon = 0\%$, 100%, 567% and 1150%, and a picture of the as-cast specimen bent through 90° without fracture is inset. Typical XRD patterns of the as-cast and as-rolled specimens are shown in Fig. 2b. Besides two broad diffraction peaks, no obvious signals from crystalline phases were detected at all values of ε. Since differential scanning calorimetry (DSC) is more sensitive than XRD to deformation-induced structural change, the corresponding DSC curves of the as-rolled specimens at 20 K min^{-1} are shown in Fig. 2c. The as-cast alloy exhibits an endothermic event, characterized by a glass transition temperature $T_g = 638$ K, followed by only one crystallization event with an onset temperature $T_x = 747$ K and a peak temperature $T_p = 753$ K. The peak temperature does not change with ε, and the enthalpy of crystallization remains at 60 J g^{-1}, indicating that crystallization is not induced by rolling. Fig. 2d shows a bright-field TEM image of the as-cast specimen, and a uniform featureless contrast was observed. The inset is a corresponding selected area electron diffraction (SAED) pattern showing a diffuse halo and no crystalline rings, which is typical for amorphous materials. Additionally, no lattice fringes and only a homogeneous maze contrast were found in the HRTEM image presented in Fig. 2e, further confirming the presence of a single amorphous phase. All the above results demonstrate that the as-cast $Zr_{64.13}Cu_{15.75}Ni_{10.12}Al_{10}$ plate of 1 mm in thickness is fully amorphous. It indicates that special attention should be paid to the effect of TEM specimen preparation on the observed microstructure [22], since Liu et al. [21] reported that bright and dark zones exist in the TEM foil prepared by ion-milling at liquid nitrogen temperature. Further TEM observation was also performed to examine the microstructure of the as-rolled specimens. Fig. 2f depicts the bright-field TEM image of the 2d-rolled specimen with the largest $\varepsilon = 971\%$. No contrast associated with structural fluctuation was observed except for a brighter shear band about 30 nm in width. The SAED pattern inset in Fig. 2f is similar to that in Fig. 2d, and only diffraction halos are observed. An HRTEM image of the region containing the shear band is shown in Fig. 2g. No lattice fringes are observed within the shear band and the matrix. Fig. 2h and i shows the magnified images of selected areas in Fig. 2g marked by I and II. All these results confirm that rolling up to $\varepsilon = 1150\%$ does not cause crystallization in $Zr_{64.13}Cu_{15.75}Ni_{10.12}Al_{10}$ BMG.

3.2. The side surface of the as-rolled specimens

Fig. 3 presents the SEM images of a side view of the as-cast and as-rolled specimens with $\varepsilon = 100\%$. The as-cast specimen shows a smooth polished surface without any visible scratches (Fig. 3a); the side surfaces of all the specimens prior to rolling deformation were examined by optical microscopy (OM) and SEM to ensure the quality of polishing. Fig. 3b shows the morphology of numerous

Please cite this article in press as: Cao QP et al. Effect of pre-existing shear bands on the tensile mechanical properties of a bulk metallic glass. Acta Mater (2009), doi:10.1016/j.actamat.2009.10.032

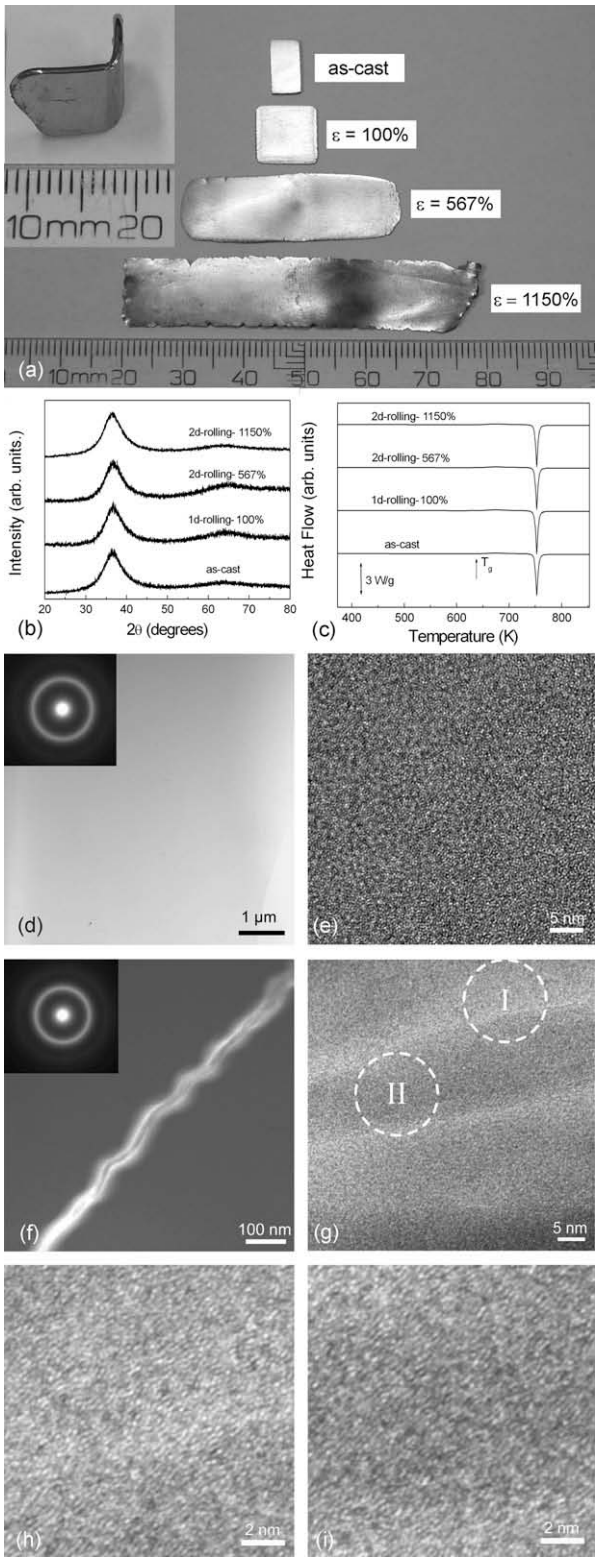

Fig. 2. (a) A picture of the as-rolled specimens with different values of ε; the inset is the shape of the as-cast specimen undergone a 90° bend. (b) XRD and (c) DSC curves of the as-rolled specimens. (d) TEM and (e) HRTEM images of the as-cast specimen; the inset in (d) is a SAED pattern. (f) TEM and (g) HRTEM images of the 2d-rolled specimen with $\varepsilon = 1150\%$; the inset in (f) is a SAED pattern. (h and i) Magnified images of the selected areas marked I and II in (g), respectively.

shear bands formed in the 1d-rolled specimen with $\varepsilon = 100\%$. There are two sets of parallel shear bands, i.e. primary and secondary shear bands, propagating across the specimen, as marked in Fig. 3b.

It is well known that primary shear bands form in the initial stage of rolling, and the angle between these shear bands and the rolling direction gradually decreases with increasing ε [13]. When these bands are significantly deviated from the maximum shear stress direction, the critical applied stress required to reactivate primary shear bands rises. If the critical stress required to initiate secondary shear bands along the maximum shear stress direction is lower than that to reactivate primary shear bands at a smaller slant angle between the shear band and the rolling direction, secondary shear banding occurs to accommodate the applied strain. Secondary shear bands cut through and interact with some of the primary shear bands, and the offset is clearly visible in Fig. 3c.

Meanwhile, a number of cracks are observed near the sites where primary and secondary shear bands intersect, caused by the mismatch of the slip movements between the primary and the secondary shear bands, and marked in Fig. 3b by a dotted circle.

It is worth noting that shear bands formed in the 1d-rolled specimen always propagate along a single direction, and no symmetric and conjugated situation exists. If two rollers and stainless steel sheets used to hold the specimens during the rolling process were perfectly symmetrical and the as-cast specimen was ideally homogeneous and isotropic, we would expect multiple shear bands to form in conjugated directions in the 1d-rolled specimens. Taking the asymmetric characteristics of shear band formation in the 1d-rolled specimen into account, we performed 2d-rolling, i.e. rotating 180° in the rolling plane after each rolling pass, in order to cause shear bands to form in conjugated directions. Fig. 3d–f shows the SEM images of the side surface taken from different parts of the 2d-rolled specimen with $\varepsilon = 100\%$. It is evident from the SEM observation that the formation of multiple shear bands in conjugated directions is introduced by 2d-rolling.

A typical SEM image of the shear bands along a single direction at higher magnification is shown in Fig. 3g. Besides primary and secondary shear bands, profuse tertiary shear bands exist between the primary and the secondary shear bands. As a result, the shear band density in the 2d-rolled specimen with $\varepsilon = 100\%$ is visibly higher in comparison to that in the 1d-rolled specimen with the same ε. Cracks are also observed near the sites where primary and secondary shear bands meet, but the size and density of cracks do not significantly increase in 2d-rolling as compared with 1d-rolling.

Fig. 3h presents the magnified image of the area selected in Fig. 3d, i.e. the junction region of shear bands in conjugated directions, where profuse shear bands in conjugated directions intersect. It is evident that the deformation of as-rolled specimens at room temperature is in the heteroge-

Please cite this article in press as: Cao QP et al. Effect of pre-existing shear bands on the tensile mechanical properties of a bulk metallic glass. Acta Mater (2009), doi:10.1016/j.actamat.2009.10.032

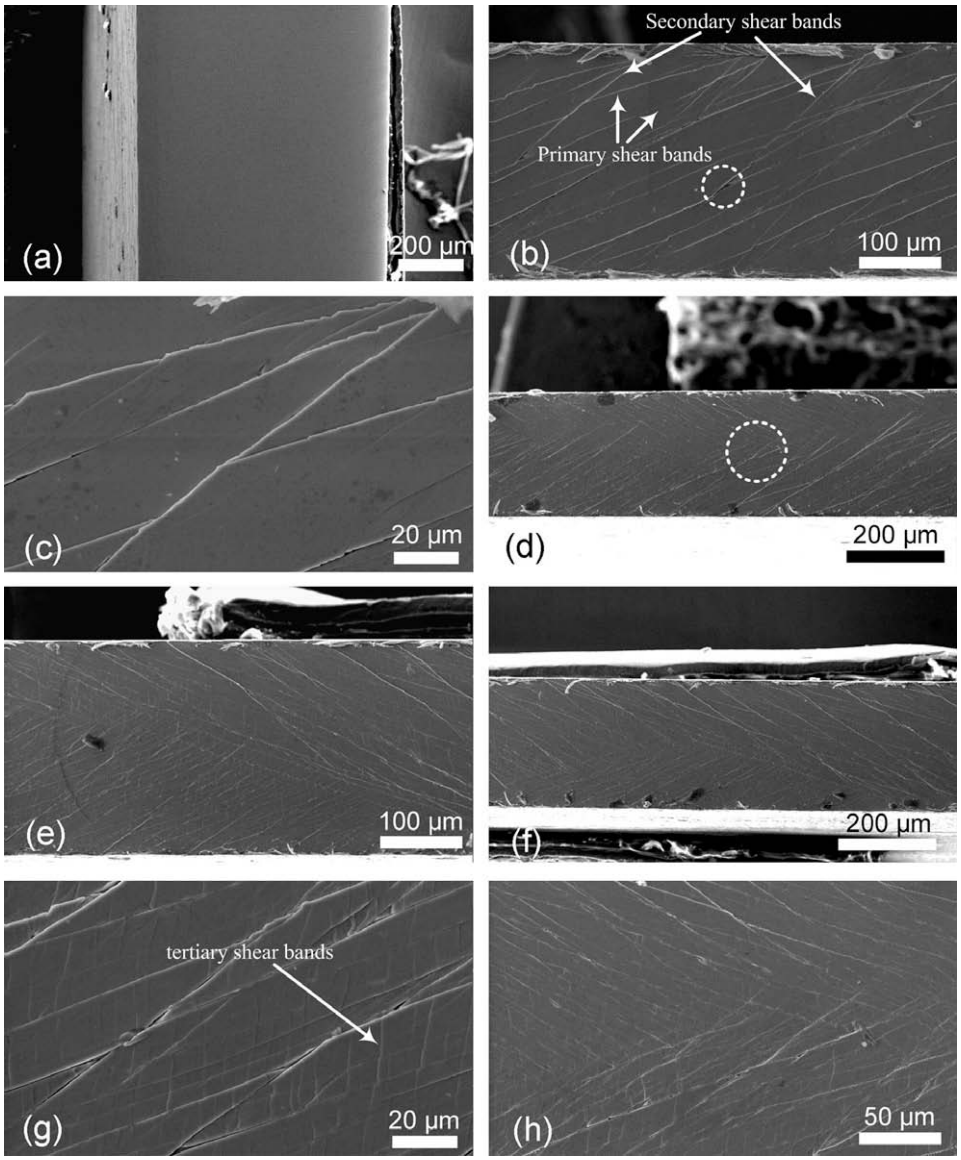

Fig. 3. Side view of the (a) as-cast, (b) 1d-rolled and (d–f) 2d-rolled specimens with $\varepsilon = 100\%$, respectively. Some cracks are observed, as marked by the dotted circle in (b). (c) Magnified image of the selected area in (b) showing the intersection between secondary and primary shear bands. (g) Magnified image of the selected area in (f) showing the existence of tertiary shear bands. (h) Magnified images of the junction region marked by dotted circle in (d).

neous region of deformation map proposed by Martinez et al. [23]. Based on the results mentioned above, changing the rolling direction can efficiently tune the orientation of shear bands from a single direction for 1d-rolling to approximately conjugated directions for 2d-rolling, meanwhile increasing the opportunity for shear bands to intersect.

3.3. Tensile tests of the as-cast and as-rolled specimens

Since pre-plastic deformation changes the microstructure of the present BMG alloy, its mechanical behavior is expected to be affected by rolling. Fig. 4a shows the tensile specimen dimensions. Tensile engineering stress–strain curves for the as-cast, 1d-rolled and 2d-rolled specimens with different ε at room temperature are presented in Fig. 4b. In order to show the results clearly, a strain interval of 1% was set between adjacent curves. Each specimen has been measured three times to ensure the reproducibility of the results. A typical stress–strain curve for each specimen state is depicted in Fig. 4c. Similar to other monolithic metallic glasses, neither yielding nor plastic strain before failure is evident for the as-cast specimen. The elastic modulus, ultimate tensile strength and elastic limit of the as-cast specimen are 77.8 ± 0.5 GPa, 1.575 ± 0.029 GPa, and $2.01 \pm 0.02\%$, respectively. The tensile elastic modulus is very close to the reported compressive value, but the fracture strength is much lower than the yield strength (1.690 GPa) in compression [21], showing obvious strength asymmetry between uniaxial tension and compression. For the 1d-rolled specimen with $\varepsilon = 100\%$, the fracture strength is 1.577 ± 0.035 GPa, which is similar to that of the as-cast

Please cite this article in press as: Cao QP et al. Effect of pre-existing shear bands on the tensile mechanical properties of a bulk metallic glass. Acta Mater (2009), doi:10.1016/j.actamat.2009.10.032

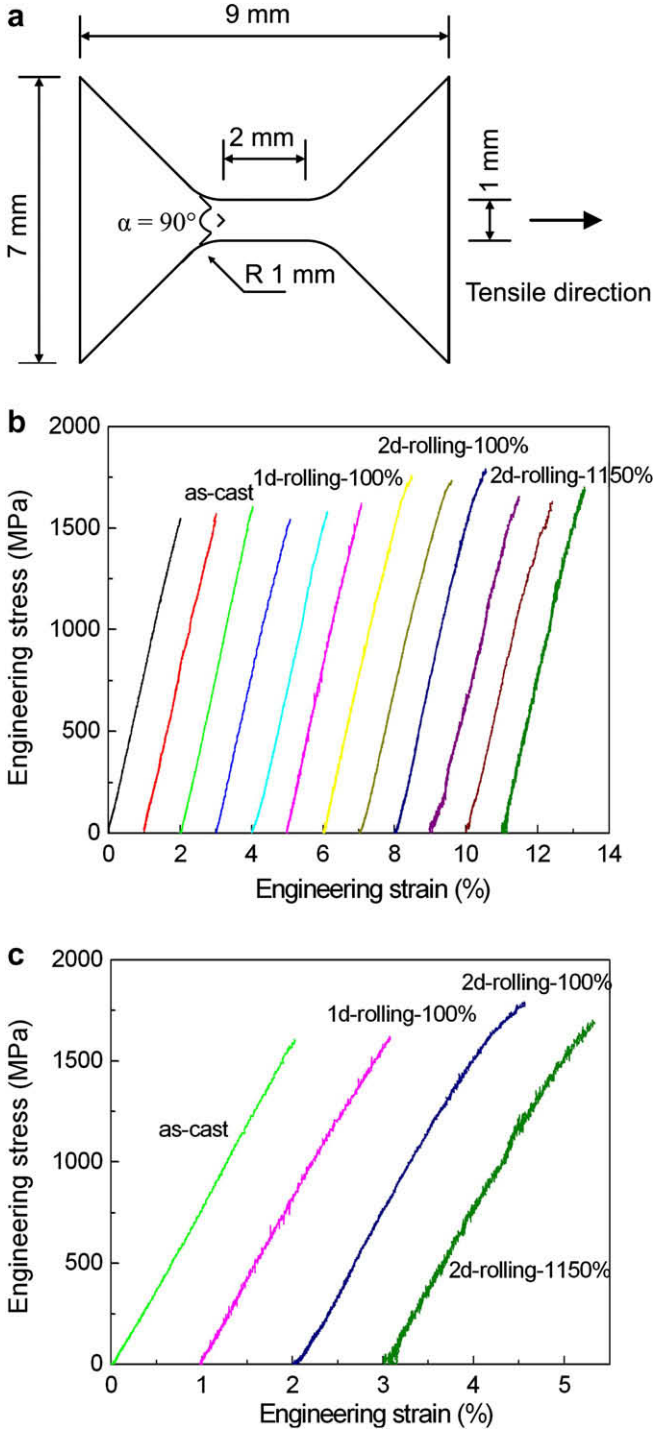

Fig. 4. (a) Tensile specimen dimensions and (b) tensile engineering stress–strain curves for the as-cast, 1d-rolled and 2d-rolled specimens with different values of ε. The curves are shifted relative to each other for clarity. (c) Typical stress–strain curves selected from (b).

specimen. A slight deviation from the elastic deformation starts at about 1.331 ± 0.040 GPa, and the elastic modulus was determined to be about 76.9 ± 1.0 GPa, which is slightly lower than that of the as-cast specimen. The lower yielding strength and elastic modulus of the as-rolled specimen as compared with that of the as-cast specimen indicate the existence of work softening, which has been observed in many deformed metallic glasses [5,24]. It can be readily understood that, since shear bands are generally considered to be weak regions with excess free volume in inhomogeneously deformed BMGs, the previously formed shear bands are the preferential sites for further plastic flow. Profuse shear bands pre-introduced into the as-rolled specimen will result in significant softening.

The elastic modulus and tensile plastic strain of the 2d-rolled specimen with $\varepsilon = 100\%$ were calculated to be 74.4 ± 2.6 GPa and $0.27 \pm 0.04\%$, respectively. Meanwhile, the yielding point is located at 1.190 ± 0.036 GPa lower than that for the 1d-rolled specimen with the same ε, which is in good accordance with its relatively high density of pre-introduced shear bands in comparison with the 1d-rolled specimen, as shown in Fig. 3. Interestingly, the fracture strength of the 2d-rolled specimen with $\varepsilon = 100\%$ is 1.754 ± 0.024 GPa, which is distinctly higher than that of the as-cast specimen and 1d-rolled specimen with $\varepsilon = 100\%$. In the 2d-rolled specimen with $\varepsilon = 100\%$, shear bands in fact appear in conjugated directions, as shown in Fig. 3d–f. Meanwhile, a number of tertiary shear bands between the primary and the secondary shear bands form as shown in Fig. 3g, which indicates that the opportunity for shear bands to intersect each other is sufficiently enhanced.

The concept that such intersection of shear bands in metallic glasses can inhibit further plastic flow and consequently enhance the plasticity and fracture stress is not entirely new. Takayama [16] and Hagiwara et al. [17] observed work-hardening phenomena in the mechanical responses of highly drawn metallic glass wires, and attributed such behavior to the intersection of shear bands. Das et al. [25] found that, after yielding in the compression tests of $Cu_{47.5}Zr_{47.5}Al_5$ BMG rod, the stress strongly increases with strain, and subsequently proposed that the intersection of shear bands decreases their sharpness, restricts catastrophic failure and increases the flow stress of the material, resulting in this "work hardening" behavior. However, their further investigations indicated that nanometer-scale structural inhomogeneity, chemical heterogeneity and/or nanocrystals exist in the microstructure of the as-cast specimen, which can promote nucleation, branching and intersection of shear bands, leading to the enhanced plasticity and the rise in flow stress with strain [26]. Therefore, the reliability of proposed work-hardening mechanisms by shear band intersection in the $Cu_{47.5}Zr_{47.5}Al_5$ specimen is largely reduced.

So far, there have been no substantial reports about work hardening by intersections of shear bands in monolithic metallic glasses subjected to other deformation modes, e.g. cold rolling, uniaxial compression and tension, except for drawing. In uniaxial compression and tension of metallic glasses, shear bands do not have much opportunity to intersect each other since the obtained global plasticity and shear band density are generally limited. When subjected to cold rolling, metallic glasses can undergo

Please cite this article in press as: Cao QP et al. Effect of pre-existing shear bands on the tensile mechanical properties of a bulk metallic glass. Acta Mater (2009), doi:10.1016/j.actamat.2009.10.032

severe plastic deformation without fracture [13,27]. However, in the previous work on as-rolled specimens, much of the focus has been on the influence of applied strain on the microstructure (e.g. structural relaxation, nanocrystallization and phase separation), shear band density and mechanical properties [4,13,15,19,22,27–29]; the effect of rolling direction on the shear band orientation and mechanical properties has seldom been involved. We noticed that, in a number of studies on the rolling effect of metallic glasses, the rolling direction was fixed and shear bands often propagated along a single direction. The intersection of shear bands was seldom observed, especially when the strain was relatively low [13]. As a result, work softening was often seen in the subsequent compression and tension tests of the as-rolled specimens, and a lower hardness values was detected in the indentation of the as-rolled specimen as compared with the as-cast specimen. Another benefit of using cold rolling as the deformation mode is that the side surfaces of the as-rolled specimen do not come into contact with the rollers. It can thus show the true morphology of shear bands induced by rolling, in contrast to drawing.

It should be noted that such work hardening in highly drawn Pd- and Co-based metallic glass wires and our as-rolled Zr-based specimens is not intrinsic strain hardening [1]. Monolithic metallic glasses generally exhibit strain softening during plastic deformation. In this work, we introduce heterogeneities (pre-existing shear bands and affected zone) into the metallic glass by rolling deformation to effectively stabilize the shear bands. The shear band densities of 1d-rolled and 2d-rolled specimens with $\varepsilon = 100\%$ have been calculated from Fig. 3 to be 0.048 ± 0.005 and 0.125 ± 0.008 μm^{-1}, respectively. Georgarakis et al. [30] found that the layer with 0.4 μm thickness around the shear band reaches the glass transition near 750 K during quasistatic compression of $Zr_{62}Cu_{15.5}Ni_{12.5}Al_{10}$ BMG. Since the composition of the glassy alloy is similar to that in this work, the volume fraction of the shear band-affected zone can be determined to be about 1.9 ± 0.2 and $5.0 \pm 0.3\%$ for the 1d-rolled and 2d-rolled specimens, respectively, with $\varepsilon = 100\%$.

Since the shear band and corresponding affected zone generally have a lower density (more free volume) and hardness compared with the matrix glass [24], such structural heterogeneity improves the plasticity. Hofmann et al. [12] and Das et al. [25] successfully prepared BMG matrix composites with good plasticity through the introduction of soft crystalline dendrites and nanometer-scale structural inhomogeneity, respectively. In this work, an important difference is that shear band-affected zone introduced by rolling as inhomogeneities is totally amorphous. Shear banding is preferentially initiated in the soft region, and the appropriate density and distribution of shear bands can efficiently inhibit shear band propagation, resulting in the formation of multiple shear bands and tensile ductility.

With the increase in ε, work-hardening behavior still exists in the 2d-rolled specimens, but the plastic strains thus obtained decrease. For the 2d-rolled specimen with $\varepsilon = 1150\%$, the elastic modulus is 71.4 ± 2.9 GPa lower than that of the 2d-rolled specimen with $\varepsilon = 100\%$ and the fracture strength is about 1.659 ± 0.034 GPa, which is lower than that of the 2d-rolled specimen with $\varepsilon = 100\%$ but higher than that of the as-cast specimen. It is clearly shown in Fig. 3 that as the rolling proceeds, the cracks on the side surfaces become more and more obvious. The size and number of cracks in the heavily deformed specimen with $\varepsilon = 1150\%$ might increase as compared with the slightly deformed specimens, resulting in premature failure and decreasing the tensile strength. Meanwhile, the intersection of shear bands in the heavily deformed specimens hinders rapid propagation and increases the fracture stress, although the specimen with $\varepsilon = 1150\%$ is too thin to determine the density of cracks and shear bands. The combination of both processes determines the final mechanical properties.

3.4. In situ SEM observation of shear band evolution under uniaxial tension

In order to understand the effect of pre-introduced shear bands with different orientations on the subsequent shear band evolution under uniaxial tension, we used in situ SEM to observe the initiation and evolution of shear bands in the as-cast and as-rolled specimens. The tensile specimen dimensions for in situ SEM measurements are the same as those for uniaxial tensile tests. All the tensile specimens were mounted on the loading stage of the scanning electron microscope, as illustrated in Fig. 5a for the as-cast specimen, and two ends of the specimen were fixed. In situ SEM observation of the tensile specimen was performed throughout the gauge region by cyclically moving the lens from mark "a" to mark "f", as shown in Fig. 5a, until the specimen failed upon loading. The images of the representative areas ("a"–"f") for the as-cast specimen before tension are shown in Fig. 5b–g, respectively. The pre-polished surfaces are quite smooth except for a few scratches and blots.

In the initial stage of tensile loading, no shear banding occurs. As the tension stress reaches 90.9% of the fracture stress of the as-cast specimen, the first shear band appears in the region "a", as presented in Fig. 5h, on a plane of around $\theta = 58°$ with respect to the tensile axis rather than the maximum shear stress plane forming an angle of 45° to the tensile axis, which has also been observed in numerous tensile experiments of BMGs and can be understood if the effect of normal stress on the shear angle is taken into account [31,32]. The inset in Fig. 5h is a twice-magnified image of the area containing the shear band. It is difficult to measure the propagation length of this shear band precisely due to its wavy curve, but the linear distance was estimated to be about 75 μm.

After several tension experiments in the present work, we observed that, when the tensile force further increases after the formation of the first shear band: (i) in most cases the first shear band formed does not propagate further and

Please cite this article in press as: Cao QP et al. Effect of pre-existing shear bands on the tensile mechanical properties of a bulk metallic glass. Acta Mater (2009), doi:10.1016/j.actamat.2009.10.032

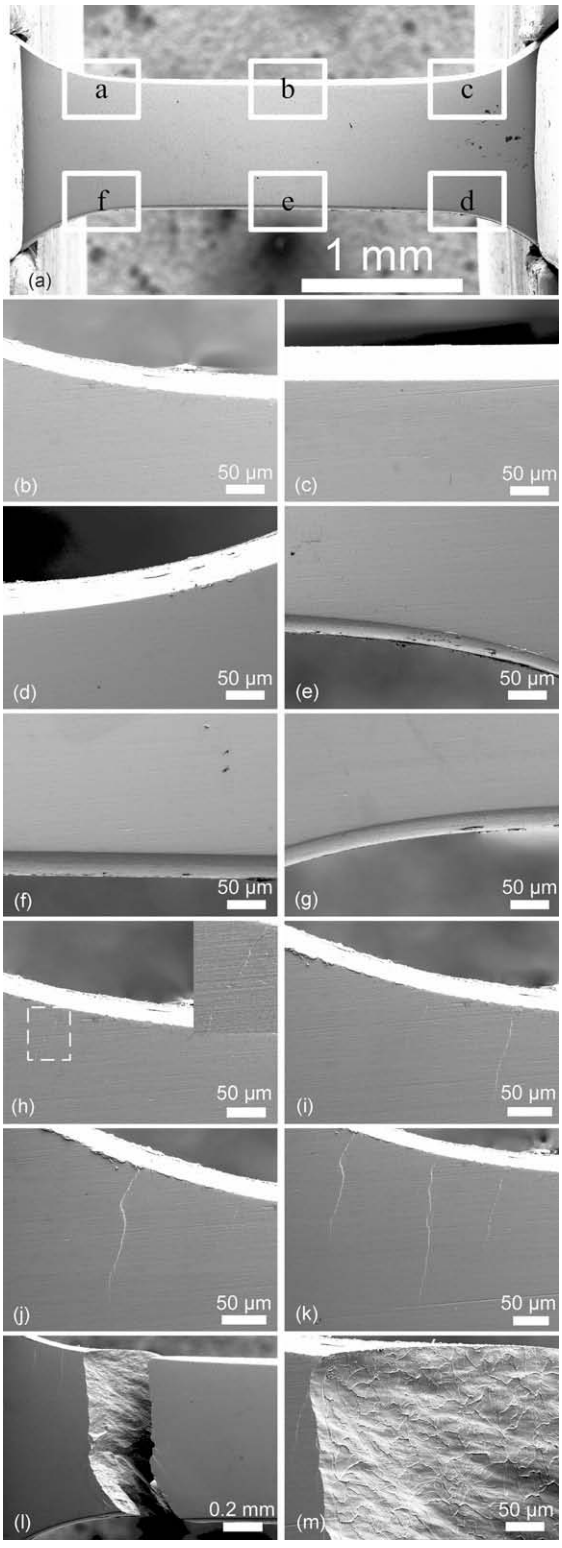

Fig. 5. The SEM images of the as-cast specimen in uniaxial tension until failure. (a) The tensile specimen is mounted on the stage; (b–g) images of the selected areas "a"–"f" in (a) before tension, respectively. (h–l) Images of shear bands when the tension stress reaches 90.9%, 93.7%, 95.7%, 97.5% and 100% of the fracture stress of the as-cast specimen, respectively. The inset in (h) is a twice-magnified image of the selected rectangular area marked by the dotted line. (m) Fracture surface of the as-cast specimen.

(ii) the second shear band, with a longer propagation length, is formed at a different location. An example is shown in Fig. 5i, which reveals the presence of the second shear band at a distance away from the first shear band of about 110 μm when the tensile stress rises to 93.7% of the fracture stress. The length of this shear band increases to about 125 μm, which is clearly longer than that of the first shear band. When the tensile stress reaches 95.7% and 97.5% of the fracture stress, the third and fourth shear bands appear, with lengths of 150 and 210 μm, as shown in Fig. 5j and k, respectively. It is evident that the initially formed shear bands do not lengthen further, even with a further increase in tensile force. At the same time, the length of a newly formed shear band increases with the applied tensile stress required for the formation of new shear band, i.e. the second shear band is longer than the first shear band, and so forth.

When the tensile stress reaches the fracture stress, the specimen catastrophically fails, as shown in Fig. 5l, and the fracture place is very close to, though not exactly the same as, the second shear band. The fracture surface is almost perpendicular to the side surface and inclined to the top surface of specimen at an angle of about 52°, determined by comparing the thickness of the specimen with the width of the fracture surface on the plate plane in the optical microscope. The fracture surface of the as-cast specimen exhibits a featureless shear plane about 20 μm in width, a characteristic vein pattern and some spheroid liquid droplets due to the melting of metallic glass caused by the instantaneous release of stored elastic energy at the moment of fracture, as shown in Fig. 5m. On the basis of the results for several tests, we concluded that the finally fractured place during uniaxial tension experiments for BMGs is most likely not at the first shear band, which indicates that propagation of the first shear band has been arrested. Consequently, nucleation of new shear bands occurs, resulting in multiple shear band formation.

SEM micrographs of the shear offset of the initial four shear bands are displayed in Fig. 6. The shear offset for the first and second shear bands is almost the same, at about 0.5 μm. For the third and fourth shear bands, the shear offset increases distinctly up to 2 μm. It is clear that the applied stress required to form shear bands increases gradually with the increase in the number of shear bands, and the larger stored elastic energy is released during the formation of the latter shear band, resulting in an increase in both the shear band length and the shear offset.

Fig. 7a–f shows the images of the representative areas ("a"–"f") of the 1d-rolled specimen with $\varepsilon = 100\%$ before tension. With the applied stress below 81.8% of the fracture stress, there are no visible changes on the surface as compared with before the tension was applied. As the applied stress reaches that critical value, multiple shear bands simultaneously form in two different parts of the specimen, as shown in Fig. 7g and h. Not only is the further propagation of existing shear bands observed when 94.0%, 96.7%

Please cite this article in press as: Cao QP et al. Effect of pre-existing shear bands on the tensile mechanical properties of a bulk metallic glass. Acta Mater (2009), doi:10.1016/j.actamat.2009.10.032

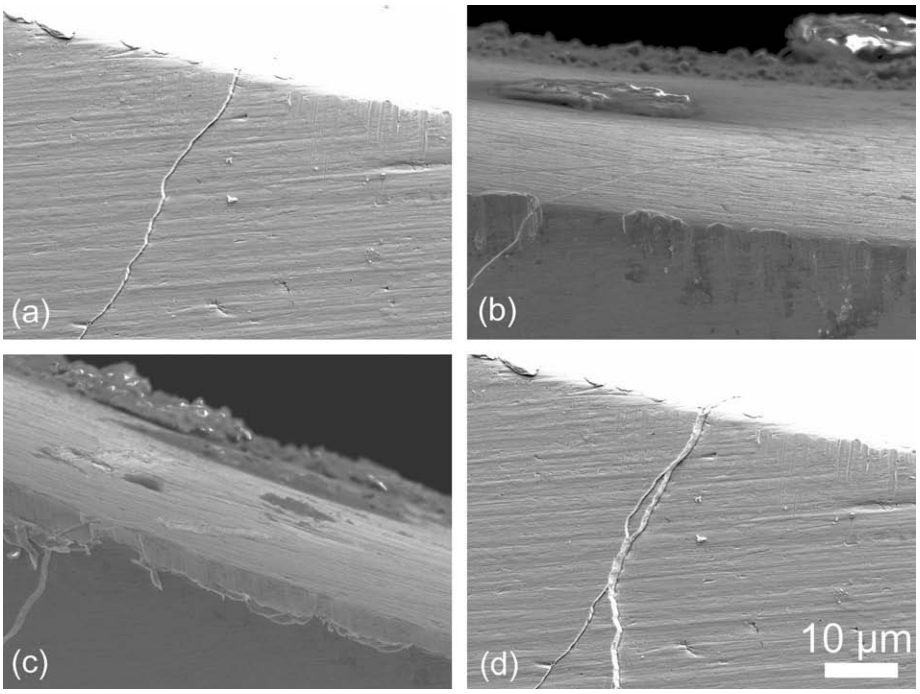

Fig. 6. SEM micrographs for shear offsets of the (a) first, (b) second, (c) third and (d) fourth shear band, respectively.

and 98.9% of the fracture stress are attained, but new shear bands also form, as shown in Fig. 7i–k, respectively. With a further rise in applied stress, final fracture of the specimen occurs, and the morphology of fractured tensile specimen is presented in Fig. 7l. The apparent yield strength, at which initial shear bands form, of the 1d-rolled specimen with $\varepsilon = 100\%$ is distinctly lower than that of the as-cast specimen, which is consistent with the results of tensile tests. Concurrent operation of pre-introduced shear bands with a single direction can promote the formation of multiple shear bands, distribute the applied strain homogeneously and facilitate plasticity, which was observed in the tensile tests of the 1d-rolled specimen with $\varepsilon = 100\%$, although this effect is not so prominent. The density of shear bands forming during tension in the 1d-rolled specimen is relatively higher than that in the as-cast specimen, as observed in in situ SEM tensile tests, further supporting this viewpoint.

Typical regions ("a"–"f") of the 2d-rolled specimen with $\varepsilon = 100\%$ before tension are shown in Fig. 8. The critical stress required to induce the initiation of the first shear band further reduces to 62.1% of the fracture stress. One shear band appears as the applied stress reaches that value, as shown in Fig. 9a. As the tension stress increases, many new shear bands appear. Fig. 9b shows the multiple shear bands forming concurrently around the first shear band, as the tensile stress reaches 74.9% of the fracture stress. The propagation and branching of the first shear band are also noticeable. Magnified images of the shear bands are illustrated in Fig. 9c and d. With the increase in tension stress up to 77.8% of the fracture stress, a number of new parallel shear bands are produced, as shown in Fig. 9e. The branching of the already formed shear bands can be seen by comparing Fig. 9f and g with Fig. 9c and d. Profuse shear bands form and propagate to accommodate the applied strain as the tension stress augments. Fig. 9h shows the morphology of tensile specimen with the tension stress at 98.7% of the fracture strength. Two major shear bands appear to cut through the whole cross-section, though this does not lead to the breakdown of the specimen. The upper and lower parts of the specimen containing shear bands at a higher magnification are shown in Fig. 9i and j, respectively. When we further increase the applied stress up to 99.6% of the fracture stress, the specimen still holds without fracture, as shown in Fig. 9k. In addition, a number of shear bands emerge simultaneously on the left-hand side of the specimen, the magnified image of which is shown in Fig. 9l. Upon further loading, the specimen ruptures. The morphology of fractured tensile specimen is shown in Fig. 9m. The fracture surface of the 2d-rolled specimen in Fig. 9n exhibits a similar feature with that of the as-cast specimen in Fig. 5m. In comparison with those in the as-cast specimen and the 1d-rolled specimen with $\varepsilon = 100\%$, the density and offsets of shear bands forming during tension in the 2d-rolled specimen are obviously higher, which is consistent with the larger plastic strain obtained in tensile test of the 2d-rolled specimen. A possible reason for this is that, since the pre-introduced shear bands can distribute the applied strain more homogeneously across the deformed region and avoid catastrophic failure, the relatively higher density of pre-introduced shear bands in the 2d-rolled specimen results in enhanced plasticity through

Please cite this article in press as: Cao QP et al. Effect of pre-existing shear bands on the tensile mechanical properties of a bulk metallic glass. Acta Mater (2009), doi:10.1016/j.actamat.2009.10.032

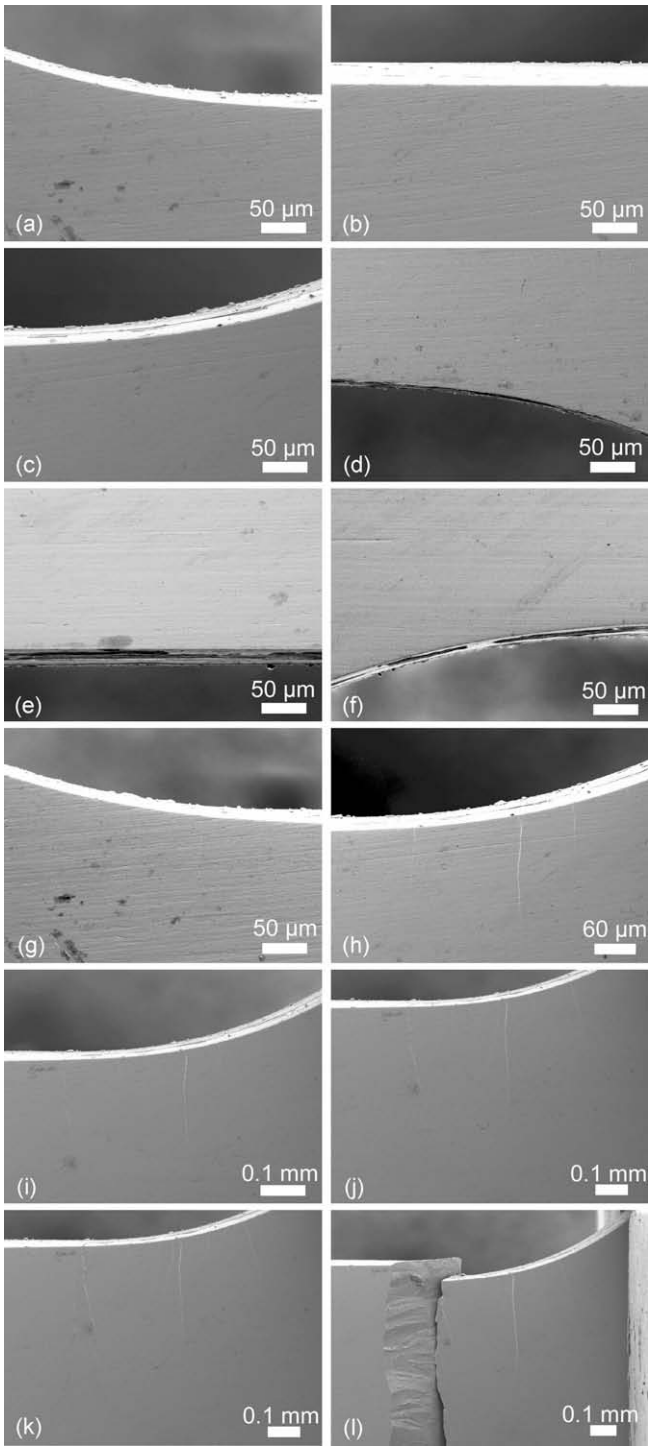

Fig. 7. (a–f) SEM images of the typical areas "a"–"f", respectively, of the 1d-rolled specimen with $\varepsilon = 100\%$ before tension. (g and h) Images of shear bands when the tension stress reaches 81.8% of the fracture stress. (i–l) Images of shear bands when 94.0%, 96.7%, 98.9% and 100% of the fracture stress is attained, respectively.

branching and multiplication of shear bands. Moreover, the interaction of shear bands in the 2d-rolled specimen is intensified as compared with the 1d-rolled specimen with the same degree of deformation, and such intersections can also restrict catastrophic failure and enhance the plasticity.

3.5. Finite element analysis and specimen geometry effect

To understand shear band formation and propagation during uniaxial tension, a detailed tension-induced stress distribution was analyzed using the finite element method. It is well known that the yielding behavior of metallic glasses depends not only on the maximum shear stress, but also on the normal stress acting on the shear plane, as indicated by tension/compression asymmetry in the yield strength and fracture angle [31–33]. The Mohr–Coulomb criterion rather than the von Mises and Tresca yield criteria can describe this situation by $\tau_y = \tau - \alpha\sigma_n$, where τ_y is the effective shear yield stress, τ is the yield stress in pure shear, α is a friction coefficient and σ_n is the stress normal to the shear plane. By simulation analysis, Lund and Schuh revealed that the Mohr–Coulomb yield criterion with $\alpha = 0.12$ captures the tension/compression asymmetry quite well, and compares favorably with the experimental data of metallic glasses [32]. Fig. 10a shows the contour of effective maximum shear stress of the as-cast BMG plate in uniaxial tension at a loading stress to be 90.9% of the tensile strength of the as-cast specimen, i.e. the stress for the formation of first shear band marking the plastic yield point, using a reasonable friction coefficient of $\alpha = 0.12$ and the Poisson's ratio of 0.377 measured in Ref. [21]. It is clear that the stress is highly concentrated in the four corners of the gauge region and nucleation of shear bands in these regions is much easier than other places during tension, which is exactly what we observed in Fig. 5.

In crystalline materials, the maximum shear stress criterion is a well accepted successful means with which to analyze the yield phenomenon. Yielding always occurs first at the location with the highest shear stress in materials when the yield stress is reached. However, Packard and Schuh [10] recently found that in the indentation experiments of metallic glasses shear banding occurs only when the yield strength is exceeded along a potential shear band path, i.e. the shear plane criterion. Using the locations and lengths of shear bands observed in the in situ SEM tensile experiment as a constraint, we analyzed the variation in effective maximum shear stress along the first three shear band paths of the as-cast specimen at the loading stress for first shear band formation, as shown in Fig. 10b. Since the fourth and fifth shear bands initiate very close to the first and second shear bands, respectively, it can be considered that there are actually three points of initiation for shear bands. It is seen that the initiation point of the first shear band possesses the highest shear stress, 1.039 GPa, in comparison to the other shear band paths. All the stresses decrease with the shear distance, and the first shear band sustains the highest stress over its entire length. If the yielding phenomenon in uniaxial tension is supposed to be determined by the shear plane criterion, one can image that the minimum of shear stress along the first shear band path (about 0.902 GPa) is just the shear yield strength of the as-cast specimen. Fig. 10c further shows the effective maximum shear stress along three shear band paths at dif-

Please cite this article in press as: Cao QP et al. Effect of pre-existing shear bands on the tensile mechanical properties of a bulk metallic glass. Acta Mater (2009), doi:10.1016/j.actamat.2009.10.032

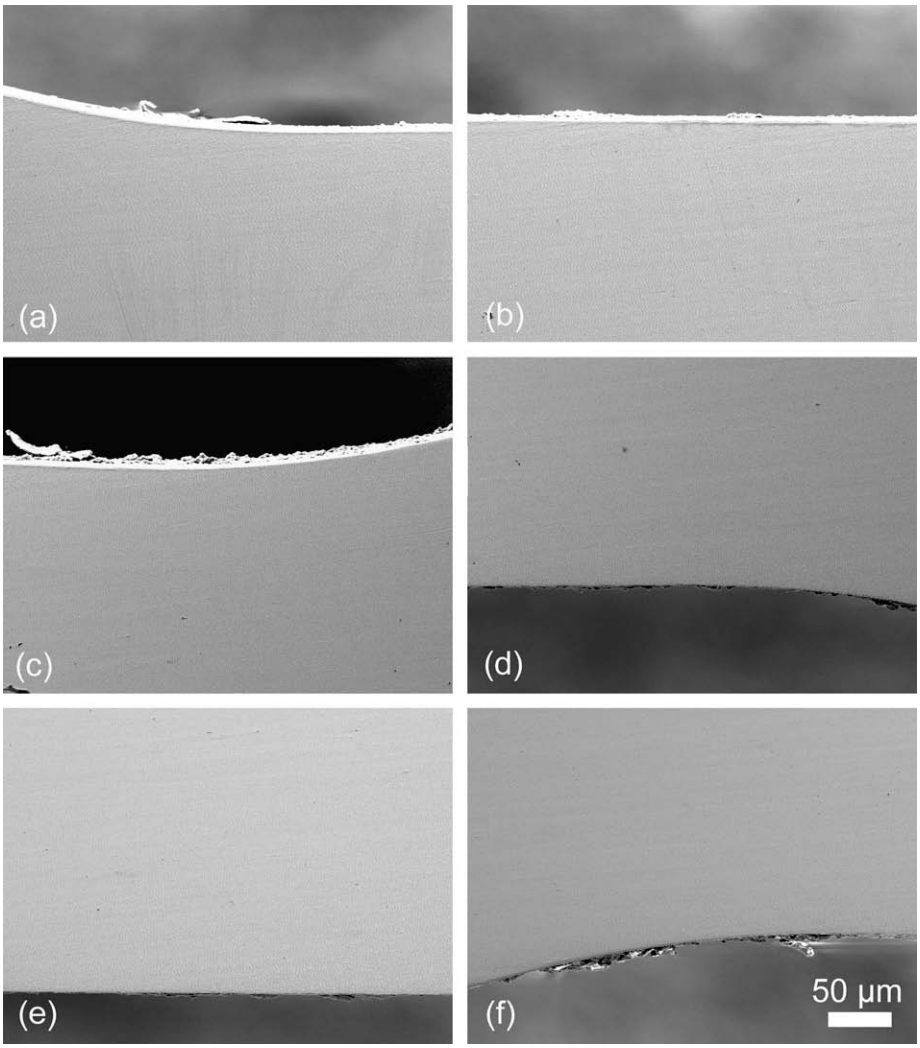

Fig. 8. (a–f) SEM images of the typical areas "a"–"f", respectively, of the 2d-rolled specimen with $\varepsilon = 100\%$ before tension.

ferent loading stresses causing the formation of these shear bands. The minimums of shear stresses along these three shear band paths are not the same. The decrease in minimum shear stress with the number of shear bands indicates that the shear plane criterion cannot describe the sequence for the formation of shear bands well since the yield strength of glassy material does not obviously vary with the location due to its homogeneous and isotropic nature. Meanwhile, shear stresses at the initiation points of three shear bands are very similar, as shown in Fig. 10c, indicating that shear banding occurs when the stress at a location reaches a certain value. It is clear that the normal-stress-modified maximum shear stress criterion rather than the shear plane criterion can describe the formation conditions of shear bands if such a certain stress is indeed the effective shear yield strength of the material. However, since the locations of the three shear bands are not in a uniaxial tensile stress state, one cannot deduce the shear yield strength τ_Y^T from the experimental tensile yield strength σ_Y^T with $\tau_Y^T = \sigma_Y^T \sin\theta(\cos\theta + \alpha \sin\theta)$, as suggested by Zhang et al. [31] and Cao et al. [34] to support this argument.

In order to cause the tensile specimen to fracture at the gauge region and obtain a uniaxial tensile stress state there, a new geometry of tensile specimen is designed and presented in Fig. 11a. Such a shape is convenient for the accurate determination of the strength of brittle materials, but the strain cannot be measured due to the small gauge length. The tension-induced stress distribution in the new shape has been analyzed, and Fig. 11b shows the contour of the effective maximum shear stress of the as-cast specimen at the ultimate tensile strength (1.476 ± 0.025 GPa), which is determined in the following in situ SEM tensile tests. It is clear that the stress in the gauge region is high and homogeneous in comparison to other regions; therefore, fracture should preferentially occur in the gauge region.

We performed in situ SEM observation of the initiation and evolution of shear bands and recorded tensile loads to calculate the tensile stress. The tensile specimen is observed by cyclically moving the lens from mark "a" to "f" in Fig. 12a, until the specimen fails upon loading. The images of the representative areas ("a"–"f") for the as-cast

Please cite this article in press as: Cao QP et al. Effect of pre-existing shear bands on the tensile mechanical properties of a bulk metallic glass. Acta Mater (2009), doi:10.1016/j.actamat.2009.10.032

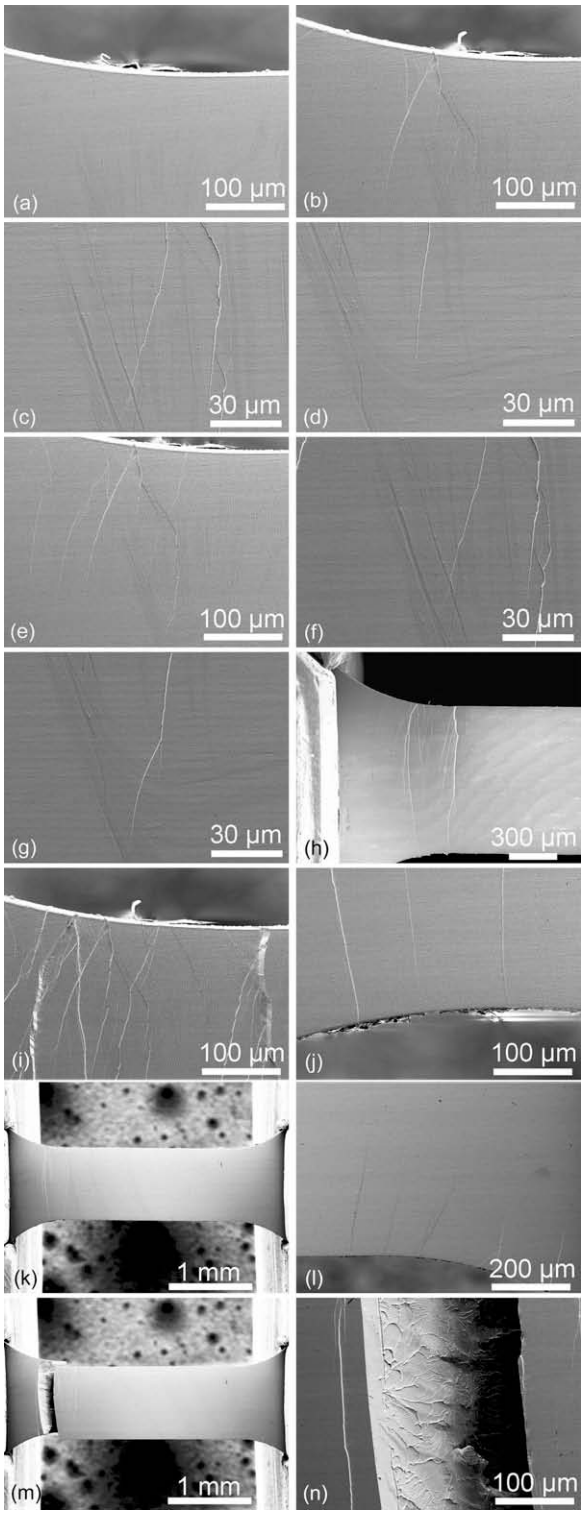

Fig. 9. (a and b) SEM images of shear bands as the tension stress reaches 62.1% and 74.9% of the fracture stress, respectively. (c and d) Magnified images of the shear bands in (b). (e) Images of shear bands when 77.8% of the fracture stress is reached. (f and g) Corresponding magnified images showing the branching of shear bands compared with (c) and (d). (h) Specimen morphology as the tension stress is 98.7% of the fracture strength. (i and j) Magnified image of the upper and lower parts of the specimen, respectively. (k and l) Specimen morphology and magnified image of the bottom left corner, respectively, as tension stress is 99.6% of the fracture strength. (m and n) Morphology of the fractured specimen and the fracture surface, respectively.

specimen before tension are shown in Fig. 12b–g, respectively. With the increase in tensile stress, no shear banding occurs before failure, as shown in Fig. 12h, and the ultimate tensile strength is 1.476 ± 0.025 GPa. Failure occurs in the middle part of the tensile specimen, and the fracture angle θ_T between the tensile axis and fracture plane is around 54°. The magnified images of the areas near the fracture plane are depicted in Fig. 12i–l, and no shear bands are observed. Fig. 12m presents an SEM micrograph observed from the fracture surface of the tensile specimen, showing typical vein patterns and the presence of some spheroid liquid droplets.

Note that under a uniaxial tensile stress state the coefficient α is directly related to the fracture angle θ_T by $\alpha = -\cos 2\theta_T/\sin 2\theta_T$ [35], and the value of α obtained for $\theta_T = 54°$ is calculated to be 0.325, which is adopted in the calculation of tension-induced stress distribution in Fig. 11b. The calculated shear fracture strength τ_F^T of the material from the experimental tensile fracture strength σ_F^T with $\tau_F^T = \sigma_F^T \sin\theta_T(\cos\theta_T + \alpha \sin\theta_T)$ is about 1.015 GPa. Since no shear bands form prior to fracture (yielding and fracture concur), τ_F^T can be considered as the effective shear yield strength of the material, which is slightly lower than the effective maximum shear stresses at the initiation points of three shear bands, 1.039 GPa, in the former specimen shape. To some extent, this discrepancy may be associated with experimental errors. In fact, it is difficult to accurately measure the fracture angle as an observation exactly perpendicular to the shear plane is required, as well as a correction for the elastic elongation of the specimen at the time of shear [36]. Therefore, it can be confirmed that, under uniaxial tension, the normal-stress-modified maximum shear stress criterion rather than the shear plane criterion can describe the conditions for the formation of shear bands in the former specimen shape.

The specimen with the new shape fails in the middle of the specimen, where the stress distribution is quite homogeneous in comparison to the edge. The effective maximum shear stress along the shear trajectory is almost the same and every point along the path is an initiation point for shear band formation. Therefore, once the yield strength is reached, every point along the shear trajectory simultaneously initiates to form a shear band, causing catastrophic failure. If shear banding occurs in the corner region, just like in the case with the former specimen shape, the effective maximum shear stress decreases along the shear band path, as shown in Fig. 10. That is to say, a shear band initiates at the highest stress region, and propagates from a high-stressed region to a low-stressed region. Such a negative stress gradient, existing in the propagation direction of shear bands, prevents the propagation of shear bands because: (i) more tensile stress is required to break up the atomic bonding and consequently to activate shear bands when they slip from high-stressed regions to areas with lower stress; and (ii) the concentrated stress is probably released in the vicinity of shear bands during propagation

Please cite this article in press as: Cao QP et al. Effect of pre-existing shear bands on the tensile mechanical properties of a bulk metallic glass. Acta Mater (2009), doi:10.1016/j.actamat.2009.10.032

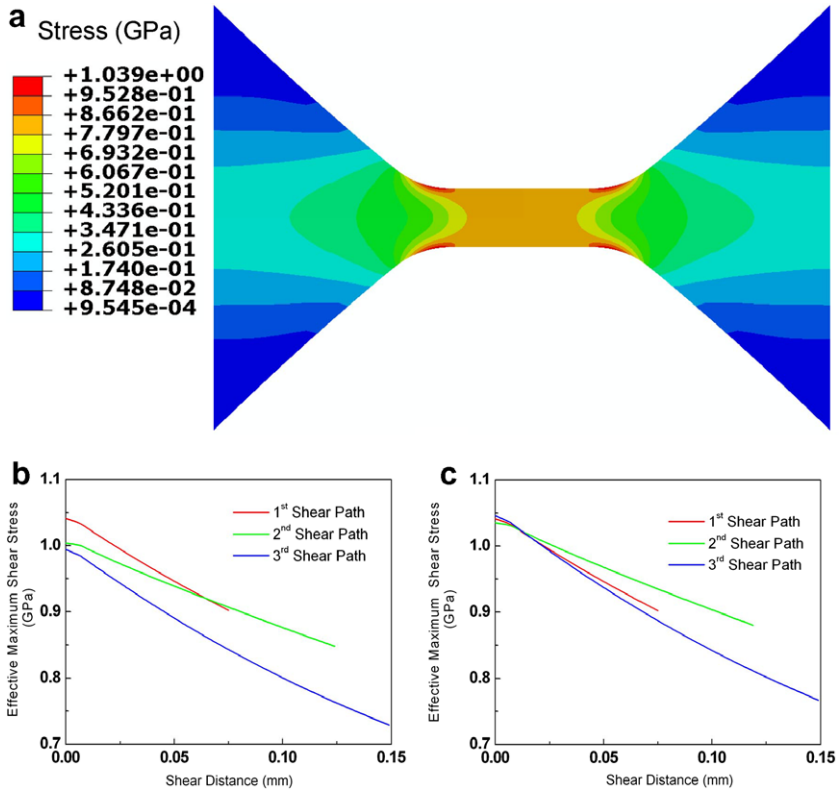

Fig. 10. (a) Contour of effective maximum shear stress of the as-cast plate in uniaxial tension at a loading stress of 90.9% of the tensile strength of the as-cast specimen, i.e. the stress level for the formation of the first shear band marking the plastic yield point, using a friction coefficient of $\alpha = 0.12$ and a Poisson's ratio of 0.377 measured in Ref. [21]. Variation of effective maximum shear stress along the first three shear band paths of the as-cast specimen (b) at the loading stress for first shear band formation and (c) at different loading stresses causing the formation of these shear bands.

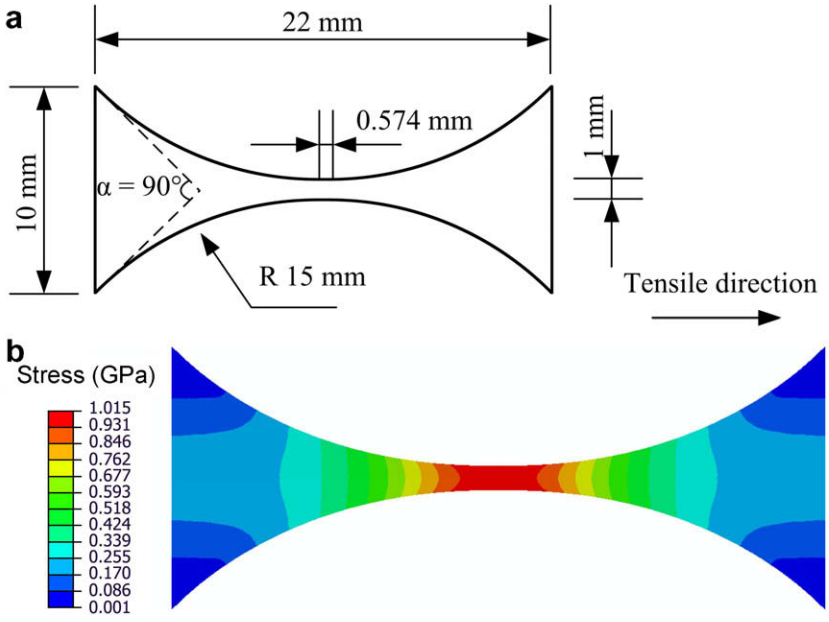

Fig. 11. (a) New geometry of the tensile specimen and (b) the contour of effective maximum shear stress of the as-cast plate in uniaxial tension at the fracture stress of the as-cast specimen, i.e. yielding and fracture concur and the fracture strength is considered to be the effective shear yield strength of the material, using a friction coefficient of $\alpha = 0.325$ and the Poisson's ratio of 0.377 measured in Ref. [21].

due to the temperature rise within shear bands caused by the dissipation of plastic work [37], although the value of the temperature rise is still under debate. For the nanoindentation of $Zr_{52.5}Cu_{17.9}Ni_{14.6}Al_{10}Ti_5$ BMG, the temperature rise

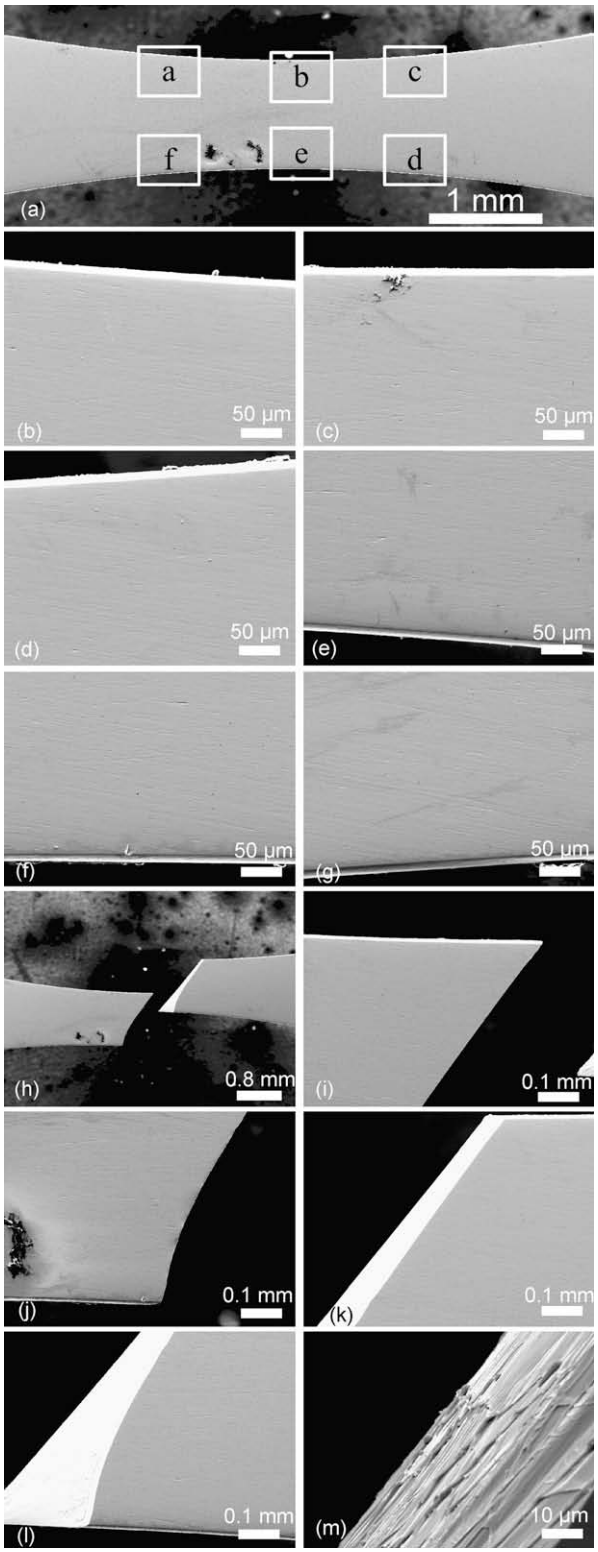

Fig. 12. The SEM images of the as-cast specimen with new geometry in uniaxial tension until failure. (a) The tensile specimen is mounted in the stage. (b–g) Images of the selected areas "a"–"f" in (a), respectively, before tension. (h) Images of the tensile specimen when the tension stress reaches the fracture stress of the as-cast specimen. (i–l) Images of different parts near fracture surface. (m) An SEM micrograph of the fracture surface of the tensile specimen.

was calculated to be just 0.05 K [38]. Under quasistatic compression of a Zr-based BMG, a temperature rise of only a few degrees was reported [39]. Recently, however, an increasing number of investigations have indicated that the temperature rise within shear bands could even be sufficiently high (up to a few thousand degrees) to cause melting [40,41]. It is reasonable that such a temperature rise may play an important role in weakening the stress field around shear bands during shearing.

In Fig. 5, what we observed experimentally is that the first-formed shear band does not propagate further as the tensile force increases, and subsequent deformation occurs by the formation of a new shear band at another location rather than reactivation of previously formed shear bands. It seems that the stress required to drive the pre-existing shear bands is higher than the stress required to nucleate a new shear band. A possible reason for this experimental observation is that, when the stress at the initiation point of the second shear band exceeds the shear yield strength, the stress in the first shear band along the potential shear path does not concentrate again above the shear yield strength owing to the weakening stress field caused by the rise in temperature. This is also the same situation for the third shear band.

In situ tensile SEM observations were also performed on the as-rolled specimens with new specimen geometry. The length of the as-cast specimen cut for rolling was 15 mm in order to satisfy the length requirement of tensile specimens for the as-rolled specimen with $\varepsilon = 100\%$. Fig. 13a–f shows the images of the representative areas ("a"–"f") of the 1d-rolled specimen with $\varepsilon = 100\%$ before tension. The ultimate tensile strength is 1.488 ± 0.032 GPa, which is similar to that of the as-cast specimen. When the tensile stress is below 96.9% of the tensile strength, no shear banding occurs. As the applied stress reaches the critical value, multiple shear bands form simultaneously in three different regions, as shown in Fig. 13g–i; the respective insets show the magnified images of selected areas containing shear bands. Shear bands formed in tension are almost perpendicular to the side surface, which is understandable in view of the orientation of the pre-introduced shear bands in the as-rolled specimens. The formation of new shear bands is observed, as shown in Fig. 13j and k, when 98.5% and 99.4% of the fracture stress is reached, respectively. The morphology of the fractured tensile specimen is presented in Fig. 13l. An SEM micrograph observed from the area near the fracture plane clearly shows the presence of shear bands, as depicted in Fig. 13m. Similar to the as-cast specimen, a typical vein pattern and a number of droplets are observed in the tensile fracture surface of the 1d-rolled specimen, as shown in Fig. 13n.

Fig. 14a–f shows the images of the representative areas ("a"–"f") of the 2d-rolled specimen with $\varepsilon = 100\%$ before tension. The measured ultimate tensile strength is 1.548 ± 0.024 GPa, which is higher than that of the as-cast specimen and the 1d-rolled specimen with $\varepsilon = 100\%$, and is

Please cite this article in press as: Cao QP et al. Effect of pre-existing shear bands on the tensile mechanical properties of a bulk metallic glass. Acta Mater (2009), doi:10.1016/j.actamat.2009.10.032

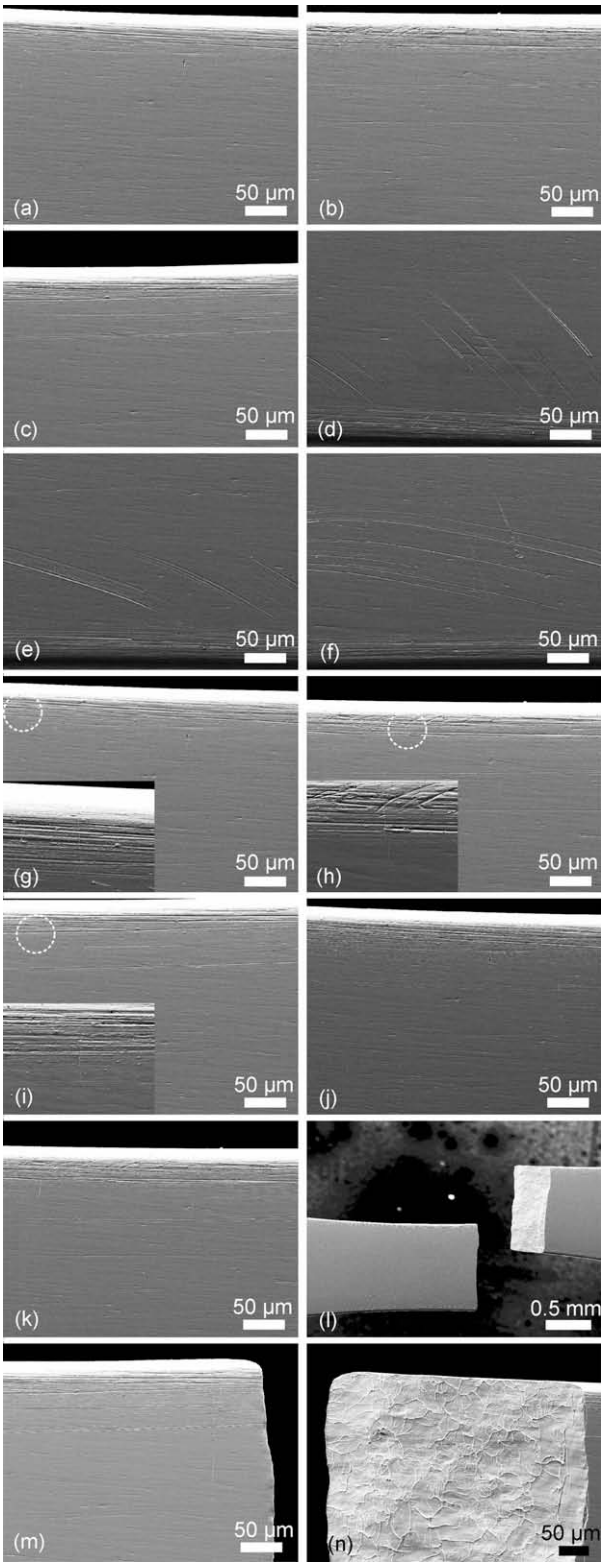

Fig. 13. (a–f) SEM images of the typical areas "a"–"f", respectively, of the 1d-rolled specimen with $\varepsilon = 100\%$ before tension. (g–i) Images of shear bands when the tension stress reaches 96.9% of tensile strength; the insets are the magnified images of the selected areas. (j and k) Images of shear bands when 98.5% and 99.4% of the fracture stress is attained, respectively. (l–n) Morphology of the fractured specimen, the micrograph of the area near the fracture plane and images of the fracture surface, respectively.

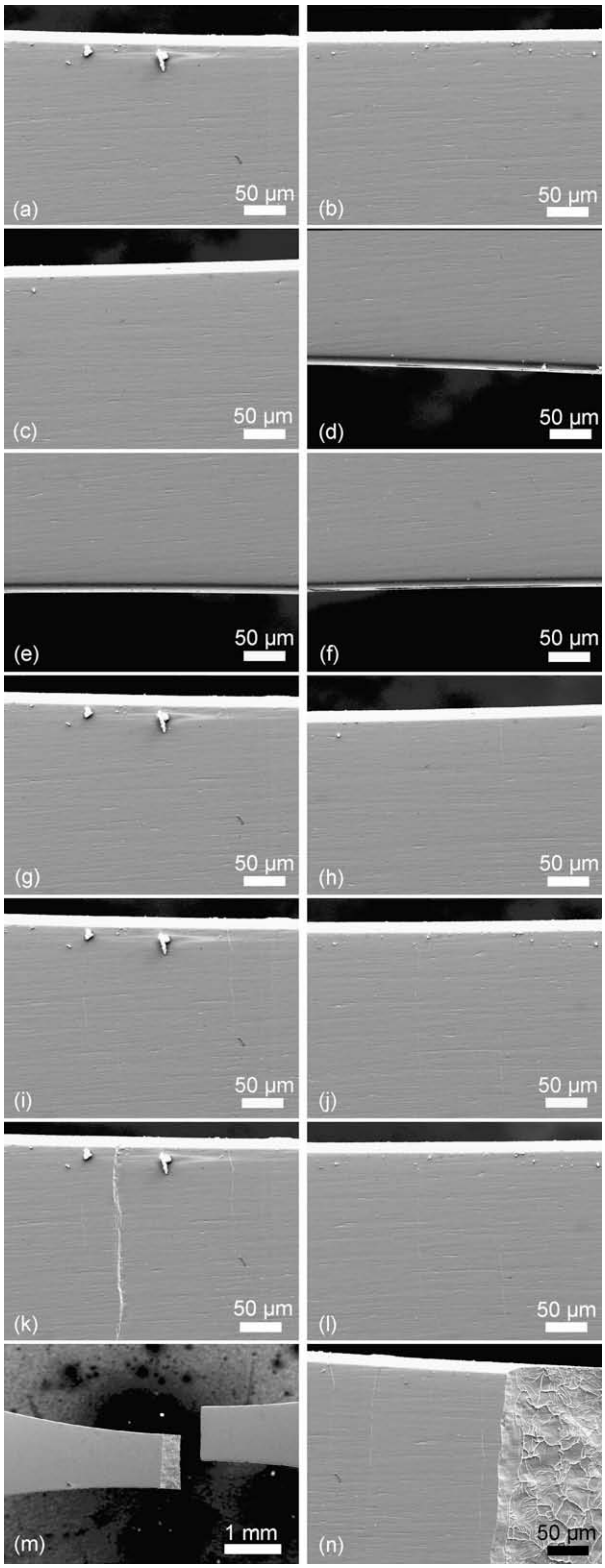

Fig. 14. (a–f) SEM images of the typical areas "a"–"f", respectively, of the 2d-rolled specimen with $\varepsilon = 100\%$ before tension. (g–l) Images of shear bands when the tension stress reaches (g and h) 89.6%, (i and j) 95.6% and (k and l) 97.4% of tensile strength, respectively. (m and n) Morphology of the fractured specimen and micrograph of the fracture surface, respectively.

Please cite this article in press as: Cao QP et al. Effect of pre-existing shear bands on the tensile mechanical properties of a bulk metallic glass. Acta Mater (2009), doi:10.1016/j.actamat.2009.10.032

in good agreement with the results obtained in the former specimen shape, further confirming the work-hardening behavior in the 2d-rolled specimen. When the tensile stress is below 89.6% of tensile strength, no shear banding occurs. As the applied stress reaches that critical value, multiple shear bands form simultaneously in two different regions, "a" and "c", as shown in Fig. 14g and h, respectively. The formation of new shear bands in the "a" and "b" regions is observed, as shown in Fig. 14i–l, when 95.6% and 97.4% of the fracture stress is attained, respectively. The morphology of the fractured tensile specimen is presented in Fig. 14m, and the fracture surface shown in Fig. 14n exhibits a feature similar to that of the as-cast and 1d-rolled specimens. The number of shear bands forming during tension in the 2d-rolled specimen is obviously higher than those in the as-cast specimen and the 1d-rolled specimen with $\varepsilon = 100\%$, which is also consistent with the larger tensile plastic strain obtained in the 2d-rolled specimen in tensile tests.

4. Conclusions

A comprehensive investigation into the mechanical response and microstructure of a $Zr_{64.13}Cu_{15.75}Ni_{10.12}Al_{10}$ BMG specimen rolled in two different directions was performed. The results allowed the following conclusions to be drawn:

(1) The as-cast plate, 1 mm thick, is fully amorphous, with good bending and rolling plasticity, and no phase transformation is observed during rolling except for shear bands, exhibiting a high mechanical stability against crystallization.
(2) Changing the rolling direction can efficiently tune the orientation of shear bands from a single direction for 1d-rolling to approximately conjugated directions for 2d-rolling, and profuse tertiary shear bands between the primary and secondary shear bands in the 2d-rolled specimen form, significantly increasing the opportunity for shear bands to intersect each other. The work-hardening behavior and obvious plastic strain of the 2d-rolled specimen with $\varepsilon = 100\%$ is clearly observed in uniaxial tension, which is further confirmed by profuse and concurrent shear band formation in in situ tensile SEM experiments.
(3) Shear bands created during rolling result in a second phase where the material has a lower density, reflected in the lower elastic modulus and yield strength of the as-rolled specimen. When spaced properly, the second phase (pre-existing shear bands) stabilizes the shear bands, leading to tensile ductility.
(4) It is revealed that under uniaxial tension the shear plane criterion cannot describe the conditions for the formation of shear bands, while the normal-stress-modified maximum shear stress criterion can.

Acknowledgements

The authors acknowledge the help of Prof. K. Hono, of the National Institute of Materials Science, Japan, with the HRTEM observations of the as-rolled specimens. Financial support from the National Natural Science Foundation of China (Grants Nos. 50701038, 50601021, 6077 6014, 60876002, 10804096, 50890174 and 10702062), the China Postdoctoral Science Foundation project fund (Grant Nos. 20070421157 and 200801451), the Zhejiang University–Helmholtz cooperation fund, the Ministry of Education of China (Program for Changjiang Scholars and the Research Fund for the Doctoral Program of Higher Education), the Department of Science and Technology of Zhejiang province and Zhejiang University is gratefully acknowledged.

References

[1] Schuh CA, Hufnagel TC, Ramamurty U. Acta Mater 2007;55:4067.
[2] Ramamurty U, Jana S, Kawamura Y, Chattopadhyay K. Acta Mater 2005;53:705.
[3] Schroers J, Johnson WL. Phys Rev Lett 2004;93:255506.
[4] Chen HS. Appl Phys Lett 1976;29:328.
[5] Bei H, Xie S, George EP. Phys Rev Lett 2006;96:105503.
[6] Spaepen F. Acta Metall 1977;25:407.
[7] Inoue A. Acta Mater 2000;48:279.
[8] Schuh CA, Nieh TG. J Mater Res 2004;19:46.
[9] Antoniou A, Bastawros A, Biner B. J Mater Res 2007;22:514.
[10] Packard CE, Schuh CA. Acta Mater 2007;55:5348.
[11] Hays CC, Kim CP, Johnson WL. Phys Rev Lett 2000;84:2901.
[12] Hofmann DC, Suh JY, Wiest A, Duan G, Lind ML, Demetriou MD, et al. Nature 2008;451:1085.
[13] Yokoyama Y. J Non-Cryst Solids 2003;316:104.
[14] Zhang Y, Wang WH, Greer AL. Nat Mater 2006;5:857.
[15] Yokoyama Y, Inoue K, Fukaura K. Mater Trans 2002;12:3199.
[16] Takayama S. Mater Sci Eng 1979;38:41.
[17] Hagiwara M, Inoue A, Masumoto T. Mater Sci Eng 1982;54:197.
[18] Hughes DA, Hansen N. Acta Mater 2000;48:2985.
[19] Cao QP, Li JF, Zhou YH, Horsewell A, Jiang JZ. Acta Mater 2006;54:4373.
[20] Lu L, Sui ML, Lu K. Science 2000;287:1463.
[21] Liu YH, Wang G, Wang RJ, Zhao DQ, Pan MX, Wang WH. Science 2007;315:1385.
[22] Chen LY, Zeng YW, Cao QP, Vainio U, Park BJ, Chen YM, et al. J Mater Res 2009;24:3116.
[23] Martinez R, Kumar G, Schroers J. Scripta Mater 2008;59:187.
[24] Jiang WH, Pinkerton FE, Atzmon M. Acta Mater 2005;53:3469.
[25] Das J, Tang MB, Kim KB, Theissmann R, Baier F, Wang WH, et al. Phys Rev Lett 2005;94:205501.
[26] Kim KB, Das J, Baier F, Tang MB, Wang WH, Eckert J. Appl Phys Lett 2006;88:051911.
[27] Park JS, Lim HK, Kim JH, Chang HJ, Kim WT, Kim DH, et al. J Non-Cryst Solids 2005;351:2142.
[28] Masumoto T, Maddin R. Mater Sci Eng 1975;19:1.
[29] Wu G, Cowlam N, Gibbs MRJ. J Mater Sci 1984;19:1374.
[30] Georgarakis K, Aljerf M, Li Y, LeMoulec A, Charlot F, Yavari AR, et al. Appl Phys Lett 2008;93:031907.
[31] Zhang ZF, Eckert J, Schultz L. Acta Mater 2003;51:1167.
[32] Lund AC, Schuh CA. Intermetallics 2004;12:1159.
[33] Donovan PE. Acta Metall 1989;37:445.
[34] Cao QP, Xu F, Liu JW, Chen LY, Wang XD, Jiang JZ, et al. J Mater Res 2009;24:2924.

Please cite this article in press as: Cao QP et al. Effect of pre-existing shear bands on the tensile mechanical properties of a bulk metallic glass. Acta Mater (2009), doi:10.1016/j.actamat.2009.10.032

[35] Vaidyanathan R, Dao M, Ravichandran G, Suresh S. Acta Mater 2001;49:3781.
[36] Lund AC, Schuh CA. Acta Mater 2003;51:5399.
[37] Chen MW. Annu Rev Mater Res 2008;38:445.
[38] Kim JJ, Choi Y, Suresh S, Argon AS. Science 2002;295:654.
[39] Wright WJ, Schwarz RB, Nix WD. Mater Sci Eng A 2001;319–321:229.
[40] Yang B, Morrison ML, Liaw PK, Buchanan RA, Wang GY, Liu CT, et al. Appl Phys Lett 2005;86:141904.
[41] Lewandowski JJ, Greer AL. Nat Mater 2006;5:15.

Please cite this article in press as: Cao QP et al. Effect of pre-existing shear bands on the tensile mechanical properties of a bulk metallic glass. Acta Mater (2009), doi:10.1016/j.actamat.2009.10.032